Available online at www.sciencedirect.com
ScienceDirect
Journal of Environmental Sciences 2012, 24(3) 520–528
JOURNAL OF ENVIRONMENTAL SCIENCES
ISSN 1001-0742
CN 11-2629/X
www.jesc.ac.cn

Comparison of dynamic adsorption/desorption characteristics of toluene on different porous materials

Weiwei Zhang[1], Zhenping Qu[1,*], Xinyong Li[1], Yi Wang[1], Ding Ma[2], Jingjing Wu[2]

1. Key Laboratory of Industrial Ecology and Environmental Engineering (MOE), School of Environmental Science and Technology, Dalian University of Technology, Dalian, Linggong 116024, China. E-mail: huiyie1984@yahoo.com.cn
2. State Key Laboratory of Catalysis, Dalian Institute of Chemical Physics, Chinese Academy of Sciences, Dalian 116023, China

Received 07 March 2011; revised 19 May 2011; accepted 25 May 2011

Abstract

Four different types of adsorbents, SBA-15, MCM-41, NaY and SiO_2, were used to study the dynamic adsorption/desorption of toluene. To further investigate the influence of pore structure on its adsorption performance, two SBA-15 samples with different microspores were also selected. It is shown that microporous material NaY has the largest adsorption capacity of 0.2873 mL/g, and the amorphous SiO_2 exhibits the least capacity of 0.1003 mL/g. MCM-41 also shows a lower break through capacity in spite of the relatively small pore diameter, because it can not provide the necessary small geometric confinement for the tiny adsorbates. However, the mesoporous SBA-15 silica with certain micropore volume shows relatively higher adsorption capacity than that of MCM-41 silica. The presence of micropores directly leads to an increase in the dynamic adsorption capacity of toluene. Although NaY has the highest adsorption capacity for toluene, its complete desorption temperature for toluene is high (> 350°C), which limits its wide application. On the contrary, mesoporous silica materials exhibits a good desorption performance for volatile organic compounds at lower temperatures. Among these materials mesoporous SBA-15 samples, with a larger amount micropores and a lower desorption temperature, are a potentially interesting adsorbent for the removal of volatile organic compounds. This behavior should been related with the best synergetic effect of mesopores and micropores.

Key words: dynamic adsorption/desorption; mesopores; micropores; toluene
DOI: 10.1016/S1001-0742(11)60751-1

Introduction

Volatile organic compounds (VOCs) are known as one of the major contributors to the formation of photochemical ozone and secondary organic aerosol (SOA), which are also considered one of the major air pollutants. Many countries have formulated relevant laws to reduce pollutant emissions and developed corresponding reduction targets (Szegedi et al., 2009). The choice of VOCs control technology depends on the actual operating conditions and the physical and chemical properties of organic compounds (Delhoménie and Heitz, 2005). Adsorption is a reliable alternative to eliminate organic compounds from industrial waste gases because of the flexibility of the system, low energy and cheap operation costs, which is favored by the majority of researchers (Russo et al., 2008; Yao et al., 2009; Akosman and Kalender, 2009). Activated carbons are generally used in many adsorption processes because of their higher adsorption capacity and low cost. However, their efficiency is limited by their sensibility at high temperatures and their difficult regeneration (Baek et al., 2004). Therefore, the most research is focused to select the adsorbent with a good stability and regeneration performance recently. New porous materials such as zeolites (Piwonski et al., 2000; Tong et al., 2008; Wang et al., 2009) and metal oxides (Agelakopoulou and Roubani-Kalantzopoulou, 2009) are proposed to be used as adsorbents for VOCs removal.

To well understand the nature of the adsorption process, the influence of pore size, surface properties, pore structure and morphology of the adsorbents on VOCs adsorption has been reported (Guillemot et al., 2007; Serrano et al., 2004; Hu et al., 2009). However, most research is focused on investigating the influences of one or two kinds of similar adsorbent on the VOCs adsorption. And few authors have reported the specific impact of pore structure of different kinds of materials in the adsorption/desorption process. Kosuge et al. (2007) have investigated the porous properties of various adsorbents and VOCs adsorption/desorption, just focusing on the pore structure and morphology of mesoporous silica. The interaction features of zeolites with adsorbent molecular are very important to understand the nature of the adsorption/desorption process.

In this article, to further study the effect of different pores (micro-and mesopores) on the dynamic adsorp-

* Corresponding author. E-mail: zhenpq@yahoo.com

tion and desorption of toluene and the synergetic effect between different pores, different types of adsorbents were selected to study the dynamic adsorption/desorption of toluene. Hydrophobic molecular sieves such as high silica materials MCM-41 are selected as adsorbent for toluene removal, which have uniform pore size, superior hydrothermal stability, high surface area, pore volume, and open pore structure. Microporous zeolite NaY and pure amorphous SiO_2 were also chosen as adsorbent, aiming to explore the effects of the different pore structure and the ordered channels on VOCs adsorption. In addition, another high silica material SBA-15 was used to study the synergetic effect of the micropores and mesopores for the adsorption/desorption of toluene. Temperature-programmed desorption (TPD) experiments were carried out to compare desorption amount and temperature for the toluene adsorbed on different adsorbent materials.

1 Experimental

1.1 Materials

High-purity aromatic hydrocarbon toluene (99.5 wt.%, Aldrich, USA) was used as adsorptive. Five kinds of porous materials were used as adsorbents. Microporous material NaY (Na_{52} $[(AlO_2)_{52}(SiO_2)_{140}]\cdot 240H_2O$, where Si/Al = 2.7) was supplied by Degussa AG, Germany. To eliminate organic impurities the zeolite was calcined in air at 510° for 12 hr. SiO_2 was supplied by Qingdao Sea Chemical Factory, China. The mesoporous materials SBA-15-1 was supplied by the Shanghai Novel Chemistry Technology Co., China. SBA-15-2 material was synthesized based on the method introduced by Zhao et al. (1998). In a typical synthesis procedure, 4.0 g of P123 (EO20PO70EO20, Aldrich, USA) surfactant and 8.50 g of tetraethyllorthosilicate (TEOS, Xilong Chemical Co., Ltd., China) were dissolved into 120 mL of 2 mol/L HCl (Beijing Chemical Plant, China) aqueous solution, after 5 min of vigorous stirring, the mixtures were stirred at 40°C for 4 hr. The mixing solution was then transferred into the Telfon reaction container (homemade) and kept it at 100°C for 48 hr. The solid material was filtrated, washed with water, dried in air at 100°C for 24 hr, and calcined at 540°C in Muffle for 8–10 hr.

For the silica MCM-41 synthesis, a detailed preparation procedure could be described as follows. A 2.4-g cetyltriethylammnonium bromide (CTAB, Tianjin Guangfu Fine Chemical Research Institute, China) and 0.48 g NaOH (Tianjin Bodi Chemical Co., Ltd., China) were mixed and stirred at room temperature until all the samples dissolved. Then, to this mixture, 12.5 mL tetraethylorthosilicate was added slowly with a vigorous stirring for 5 hr. The mixture was transferred into a teflon-lined autoclave and synthesized at 110°C for 48 hr under autogenous pressure. After the autoclave was cooled down to room temperature, the as-synthesized MCM-41 material was filtered, washed with deionized water, air-dried, and finally calcined in air at 550°C for 8 hr with a heating rate of 1°C min.

1.2 Characterization of adsorbents

Small-angle X-ray diffraction (XRD) patterns were recorded on a D/max powder diffraction system using Cu $K\alpha$ radiation (λ = 0.15418 nm) in the 2θ range of 0.5–10° with a scanning rate of 0.5°/min.

The N_2 isotherms were measured by AUTOSORB-1 (Quantachrome, USA) at 77.35 K. Prior to N_2 adsorption analysis; the samples were degassed at 573 K for 4 hr. The BET surface areas were calculated based on the linear part of the BET plot (P/P_0: 0.05–0.3). The total pore volumes were estimated according to nitrogen uptake at a relative pressure (P/P_0) of ca. 0.990. The pore size distribution and pore diameter were derived from the desorption branch of the N_2 isotherms using Barrett-Joyner-Halenda method for SBA-15-1, SBA-15-2, MCM-41 and SiO_2 samples, and by Saito-Foley method for NaY sample.

Scanning electron microscope (SEM) was performed on a JEOL JSM-6360 scanning electron microscope (USA) operating at an acceleration voltage of 20–30 kV.

1.3 Dynamic adsorption and desorption experiments

The samples were crushed and sieved between 20 and 40 meshes. About 100–200 mg of pelletized sample was loaded in the absorption bed (U-type tube), and the samples were heated at 200°C for 5 hr under He flow to remove the physically adsorbed water and small organic impurities adsorbed in pores. The dynamic adsorption and desorption experiment was carried out on the experimental set-up, as shown in Fig. 1. Toluene was carried out by Argon (99.99%, Guangming Research & Design Institute of Chemical Industry, China) in a tube (2.00 cm o.d. Pyrex) and diluted with 30% O_2/Ar. An ice bed was used to control the concentration of the toluene. The gas flow rate was controlled by mass flow controllers (Beijing Seven Star Electronics Co., Ltd., China). Fresh absorbent was placed in the tubular reactor (1.00 cm o.d. Pyrex) and adsorbed at room temperature (30°C), which was monitored by a temperature controller (Xiamen Yuguang Automation Technology Co., Ltd., China). Both inlet and

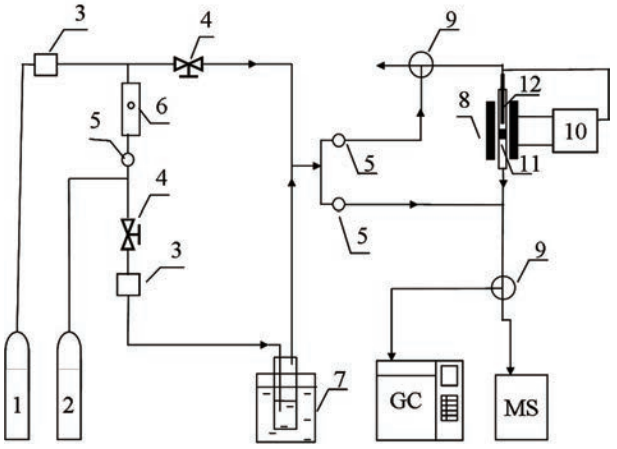

Fig. 1 Experimental setup for VOCs absorption experiments. (1) mixed-gas 30% O_2/Ar cylinder; (2) Ar cylinder; (3) mass flow controller; (4) stopvalve; (5) throttling valve; (6) rotermeter; (7) ice bath; (8) heater; (9) three-way ball valve; (10) temperature controller; (11) adsorbent bed; (12) thermocouple.

outlet gas samples were analyzed on-line using Agilent 7890 gas chromatograph (GC) equipped with a flame ionization detector (USA).

In the present experiments, the inlet stream for dynamic adsorption was a mixture of 0.27 mg/L toluene in air carrier with a flow rate of 50 mL/min. The breakthrough curves for each adsorbent were acquired at room temperature and the adsorption capacities could be determined by calculating the areas from breakthrough curves. The TPD experiments were also conducted on the above experimental set-up. The reversibly adsorbed toluene was then removed by treatment in He flow. The completion of the physical desorption process was confirmed by the recovery of the baseline of the GC or MS (mass spectrometer). The TPD tests were carried out by heating the sample with a ramp of 5°C/min with a constant He flow. The temperature of the maximum peak in the desorption curve (T_d) and the overall amount of adsorbate retained and desorbed by the adsorbent samples were obtained by comparing the peak area of desorption peak in each experiment.

2 Results and discussion

2.1 XRD

Figure 2 shows XRD patterns of the five samples. NaY sample shows the diffraction peaks at 6.2°, 10.1°, 11.9°, 15.6° and 20.3°, which corresponds to the typical X-ray diffraction pattern of NaY zeolite (Huang et al., 2010). The XRD pattern of SiO_2 only shows an obvious wide diffraction at 22.56°, indicating the amorphous structure of mesoporous materials. SBA-15 and MCM-41 exhibit the similar XRD patterns, with intense (100) diffraction peaks and two or more well-resolved peaks (100, 110, 200), which are indexed as 2D hexagonal symmetry. The corresponding XRD peaks of MCM-41 are shifted to a higher diffraction angle because of the smaller mesopore compared with that of SBA-15. Compared to SBA-15-1 sample, the intensity of all peaks for SBA-15-2 sample is considerably stronger and the peak position is shifted to lower 2θ value slightly, which might be due to the increase in the crystallinity and crystal size of the SBA-15-2 material.

Figure 3 exhibits SEM images of the four different materials. The microscopic morphology of SBA-15-1 is similar to SBA-15-2, which was not shown here. As can be seen in Fig. 3a, NaY consists of a large amount of small spherical particles, whose surface is not smooth with the size about 2 μm. No specific morphology of MCM-41 and SiO_2 can be seen in Fig. 3b and d, respectively, they were irregular in shape. The morphology of SBA-15-2 materials (Fig. 3c) is made up of more fibers in 20–30 μm length.

2.2 Pore structures

Figure 4 illustrates the N_2 adsorption-desorption isotherms and the pore size distributions for the five different samples, different textural properties, mainly differing in pore size and pore volumes, are found, as shown in Table 1.

All of them are pure silica materials except for NaY. Likewise, they present a surface area with values around 530–610 m^2/g. The values of the total pore volumes,

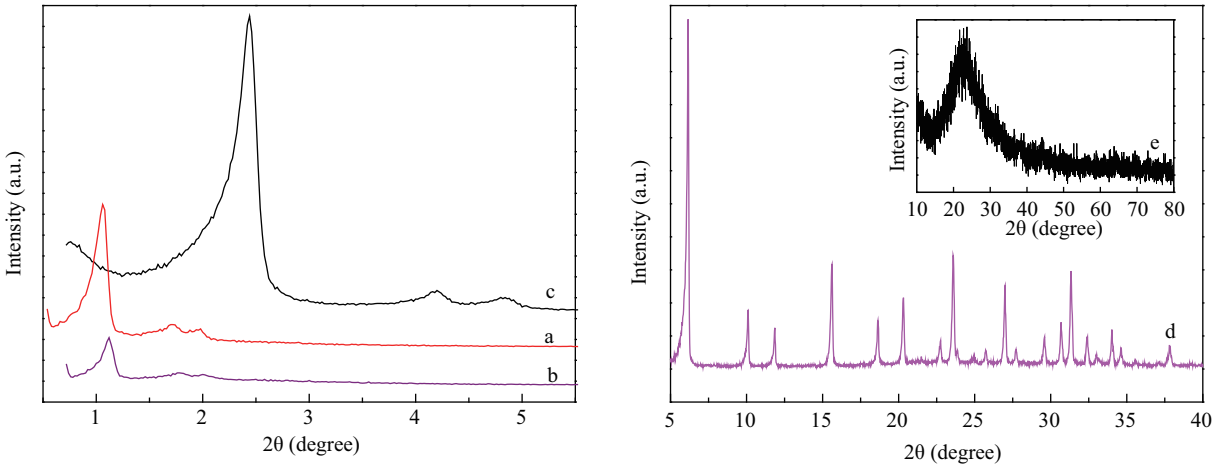

Fig. 2 X-ray diffraction patterns of SBA-15-2 (line a), SBA-15-1 (line b), MCM-41 (line c), NaY (lien d) and SiO_2 (line e).

Table 1 Structure properties of various molecular sieves

Sample	N_2 sorption				Adsorption capacity (mL/g)
	S_{BET} (m^2/g)	V_{total} (mL/g)	V_{micro} (mL/g)	D_{pore} (nm)	
SBA-15-1	612	1.00	0.05	5.60	0.17
SBA-15-2	596	0.84	0.06	6.55	0.22
MCM-41	538	0.64	–	2.38	0.15
NaY	544	0.42	0.26	0.83	0.28
SiO_2	558	0.80	–	4.33	0.10

S_{BET}: multipore surface area; V_{total}, V_{micro}: primary total pore and microporous volume evaluated by the *t*-plot method, respectively; D_{pore}: Barrett-Joyner-Halenda mesopore diameter calculated from the desorption branch.
D_{pore} of NaY was evaluated by the Saito-Foley method.

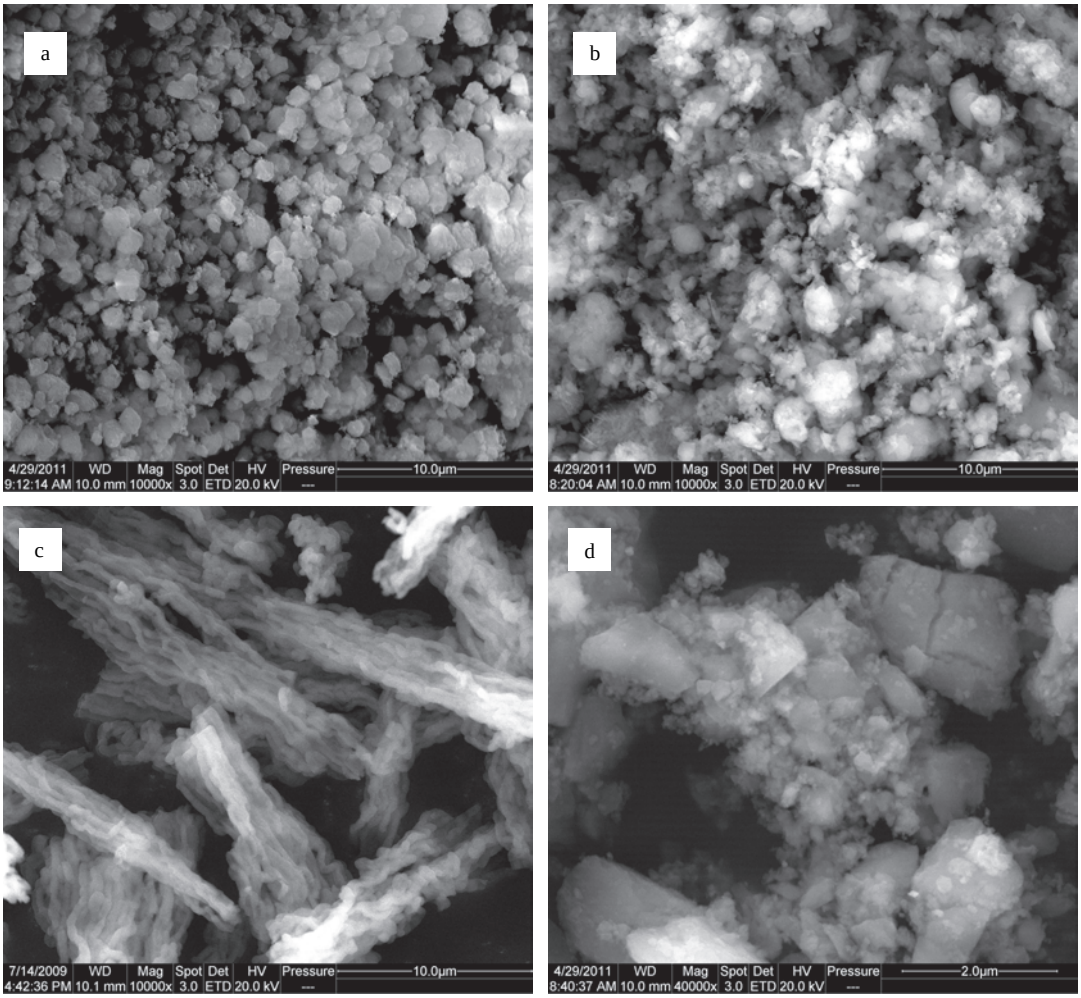

Fig. 3 SEM images of NaY (a), MCM-41 (b), SBA-15-2 (c) and SiO_2 (d).

determined from the plateau of the isotherm, are also remarkable, in the range of 0.42–1.00 mL/g. SBA-15, MCM-41 and SiO_2 are similar in shape to IV type isotherm with type H1 hysteresis loops according to the IUPAC nomenclature, typical of mesoporous materials with 1D cylindrical channel for the first two materials (Gregg and Sing, 1982). NaY, SBA-15-1 and SBA-15-2 show a steep nitrogen uptake at very low relative pressures (P/P_0 = 0.02), which is corresponding to the filling of micropores. Larger micropore volume of NaY sample results in a higher N_2 adsorption capacity at low pressures. An obvious type H4 hysteresis loop (P/P_0: 0.70–0.95) is observed for NaY, which is attributed to the filling of slit-shaped intercrystal mesopores and macropores, the former is arisen from the packing of zeolite nanocrystals and the latter is formed by the packing of aggregated particles (Huang et al., 2010). It can be clearly found that SBA-15-1 and SBA-15-2 show higher N_2 adsorption capacity at high pressures, which is due to their larger V_{total} (Table 1).

There is a sharp increase for the N_2 uptake (P/P_0: 0.2–0.3) for MCM-41 sample, which is associated with capillary condensation taking place in mesopores, and the appearance of the hysteresis loop at P/P_0: 0.48–0.96 indicates that the particle clearance hole on the sample obviously affects the gas adsorption/desorption process. The similar capillary condensation step is also observed for SBA-15 and SiO_2, but their inflection point is located at a higher P/P_0.

The appearance of the uplift curve at diameter lower than 2.5 nm for SBA-15 samples indicates the presence of microspores structure (Impéror-Clerc et al., 2000). The SBA-15-1 sample shows higher BET surface area, pore diameter and total pore volume than the other samples, but its micropore volume (0.05 mL/g) is less than that of SBA-15-2 (0.06 mL/g) and NaY samples (0.26 mL/g). SBA-15 mesoporous silica particles clearly shows a "bimodal pore system" consisting of longer 1D mesopore channels connected by complementary micropores (Kosuge et al., 2007). The formation of the complementary micropore seems to be related with the hydrophilic nature of EO-blocks of the triblock copolymer template and its incorporation in the pore walls (Ryoo et al., 2000). The presence of microporosity and the connectivity of the uniform mesopores of polymer templated silica gives a significant impact on the potential applications of these remarkable materials.

2.3 Dynamic adsorption/desorption behavior

Figure 5 shows the toluene adsorption breakthrough curves of different adsorbents. The curves can be divided into three stages, in the first stage, toluene adsorption was almost complete, the organic components of the exhaust

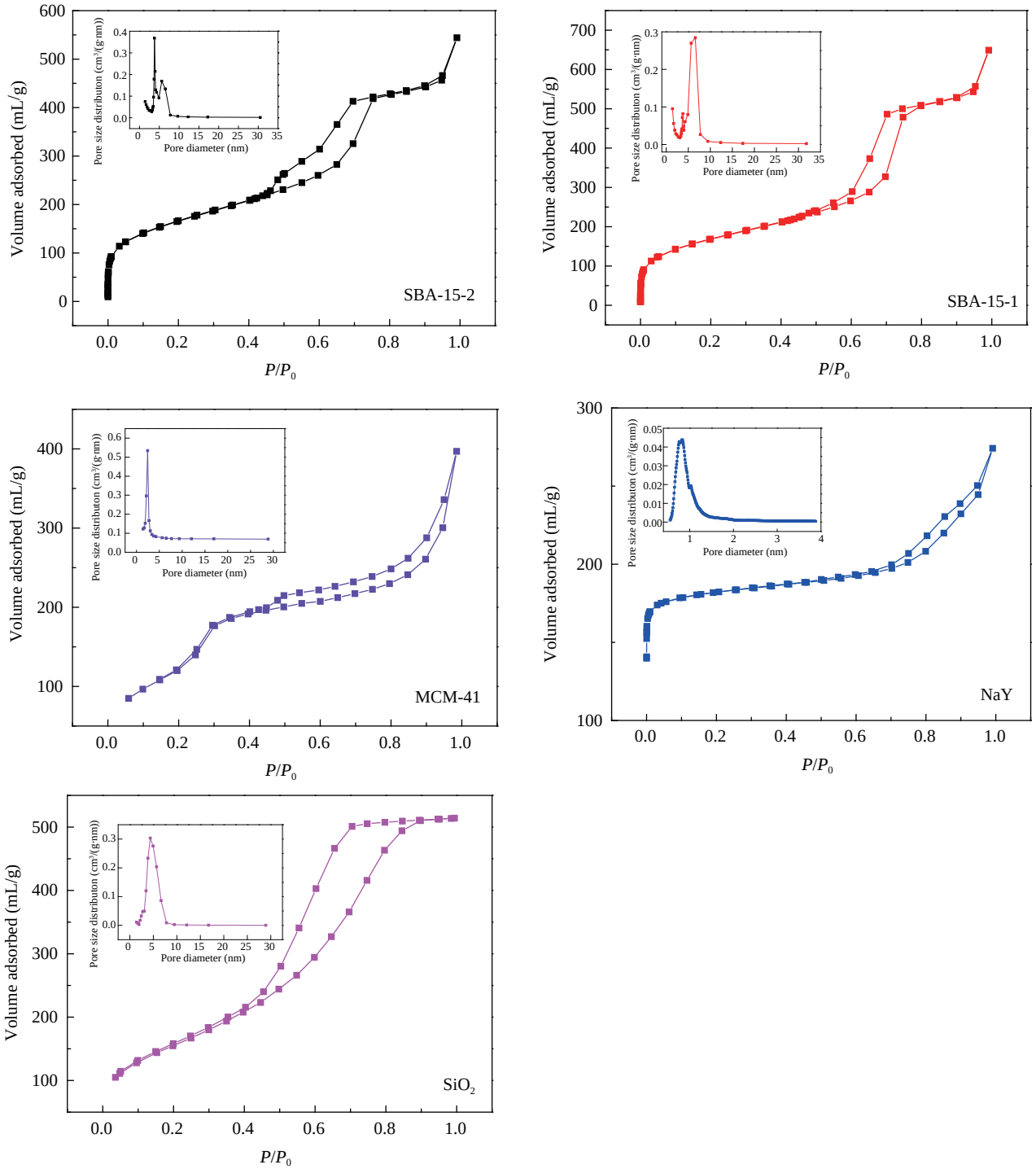

Fig. 4 N_2 adsorption-desorption isotherms and pore size distributions (insets) of the porous samples.

are close to zero, and the breakthrough curves are close to a straight line. During the second stage, the concentration of the toluene slowly reaches the breakthrough point, and the outlet toluene concentration is significant increased with the extension of adsorption time, then the outlet concentration rise in an S-shaped curve to the inlet concentration, which reaches the third stage. In general, the longer of the breakthrough time indicates a better dynamic adsorption capacity. Among the selected adsorbents, NaY showed a long breakthrough time compared with other porous materials, nearly 70 min. The shortest breakthrough time was observed on pure mesoporous MCM-41, only 10 min, however, it needs the longest time to reach adsorption equilibrium. For the other three adsorbents, the breakthrough time is the following sequence, SBA-15-2 > SBA-15-1 > SiO_2. The corresponding toluene adsorption amounts for different adsorbents are shown in Table 1. The adsorption capacity for toluene, of NaY, SBA-15-1, SBA-15-2, MCM-41 and SiO_2, is 0.28, 0.17, 0.22, 0.15 and 0.10 mL/g, respectively. It indicates that absorbents with better porous parameters (surface area and pore volume) do not necessarily show a larger breakthrough capacity. Although previous study demonstrated that adsorbed toluene was always quite close to the porosity measured by nitrogen

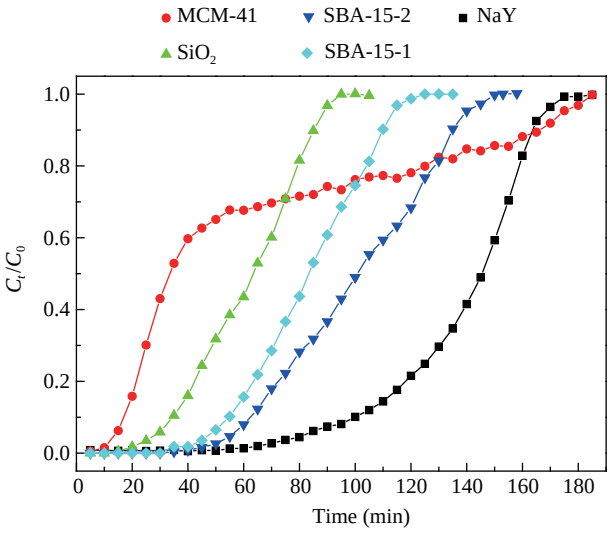

Fig. 5 Adsorption breakthrough curves of toluene over SBA-15-2, SBA-15-1, MCM-41, NaY and SiO_2.

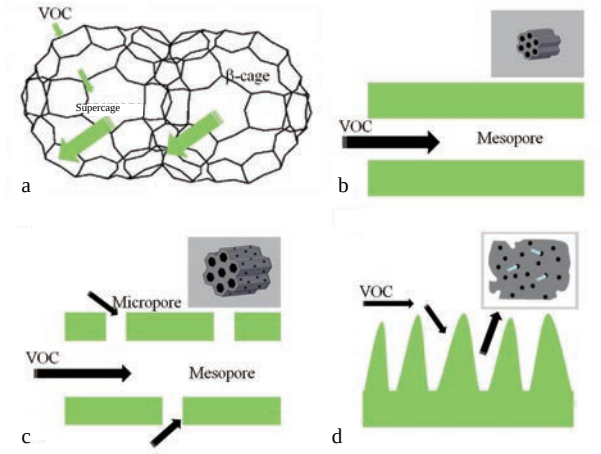

Scheme 1 Schematic drawing of the structure units of the different materials: (a) NaY; (b) MCM-41; (c) SBA-15 and (d) SiO_2. All arrows represented the diffusion direction of the VOC, and it did not represent the molecule size. All of the schemes only represented the unit structure of each material.

physical experiment (Ravikovitch et al., 2006). However, it can be noted that some difference appears in the presence of micropores with size comparable or smaller than the diameter of toluene molecules from Figs. 4, 5 and Table 1. The macroscopic morphologies of adsorption materials were shown to be an important factor in attaining superior adsorption performance. As shown in Fig. 3 and Table 1, the material with specific morphology (SBA-15 and NaY) showed a better adsorption capacity, however the influence was not obvious in present study. In addition, although the macroscopic morphologies of fibers SBA-15 sample was similar, the adsorption capacity (0.54 mL/g) of SBA-15-2 obtained by Kosuge et al. (2007) was higher than the values obtained in this study, which should be due to the shorter fibers length and lower micropore volume. The present results obtained reveal the volume of micropores was an important parameter for the adsorption of VOCs at low concentrations and are in agreement with previous literature regarding the adsorption of VOCs (Lillo-Ródenas MA et al., 2002). The amount of adsorbed toluene is linearly correlated to the micropore volume, and the presence of micropores directly leads to an increase in the dynamic adsorption capacity of VOCs (Hua et al., 2009). The lower toluene volume obtained from dynamic process as compared to N_2 is most likely due to the molecular sieving effect and the relatively low micropore amounts in the porous materials.

The schematic drawing of the structure units of the different materials are showed in Scheme 1. Y-type zeolite is a natural mineral zeolite with framework of octahedral structure, β-cage is the structural element (diameter of 0.24 nm). The adjacent β-cages are connected by cubic column, forming a super-cage structure and three-dimensional pore system (Scheme 1a) (Ghorai, 2010). Super-cage contains four twelve-membered ring orifice according to the tetrahedral orientation, diameter of the ring orifice is 0.74 nm × 0.7 nm, whose size is similar to the molecular size of toluene (0.65/0.89 nm), resulting in the enhancement of dispersion interactions in the narrow pore spaces even at very low pressures (Cheng and Reinhard, 2006). In addition, the alkaline cation acted as a Lewis acid to form a strong interaction with π electrons in the case of aromatic hydrocarbons adsorption (Choudhary et al., 1990; Otremba and Zajdel, 1993; Su and Norberg, 2000) due to the sodium cation distribution in NaY cages (Marti' et al., 1977). The methyl of toluene can also enter into the β-cage and the three dimensional pore of NaY zeolite, the better adsorption capacity for toluene on NaY can also partly be attributed to the molecular sieving effect and the existing of some sodium cations.

MCM-41 is a mesoporous material with a regular channels and a pore diameter of 2.38 nm, being close to the pore size of the micropores, as shown in Scheme 1b. The adsorption performance of MCM-41 for a low-concentration VOC stream has been known to be improved when the pore-opening size is tailored to be in the microporous region, while the pore volume is significantly maintained (Hu et al., 2001). No smaller secondary holes are presented in MCM-41 sample. It has been known from Fig. 5 that it does not show an ideal adsorption breakthrough curve, and it exhibits a characteristic two-step curve. Its adsorption capacity for toluene is only 0.15 mL/g. This may be due to its single mesopore, longer channel and relatively smaller pore diameter compared with SBA-15. And the molecular diffusion resistance is also enhanced. The first step for toluene adsorption (the first 40 min of adsorption with a faster diffusion rate) on MCM-41 is associated with the open cylindrical channels of the mesopores, which is conducive to the diffusion of toluene molecules. The second step with a slower diffusion rate should be related with the resistance caused by adsorbed molecules. SiO_2 is a typical amorphous silica material, which has no regular channels (shown in Scheme 1d). A disordered structure and weak binding of organic compounds results in its low adsorption capacity.

SBA-15 shows the two-dimensional (2-D) hexagonal *p6mm* symmetry and channel-type mesopores, which is similar to MCM-41. And it has also been found that the mesopores in SBA-15 are interconnected by the presence

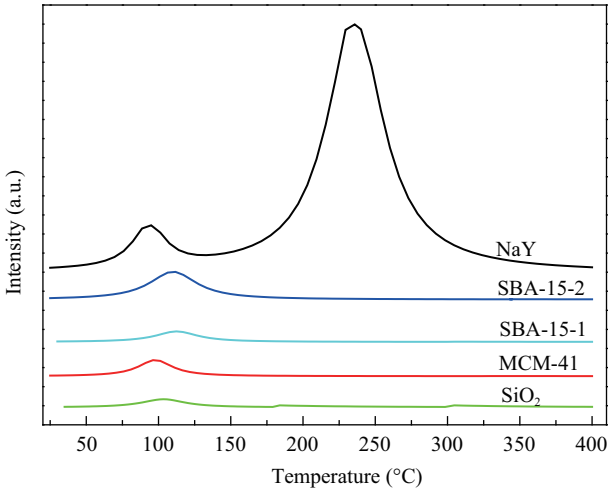

Fig. 6 Temperature-programmed desorption (TPD) of toluene over SBA-15-2, SBA-15-1, MCM-41, NaY and SiO_2.

of micropores across the silica walls, as shown in Scheme 1c (Impéror-Clerc et al., 2000; Galarneau et al., 2003). SBA-15 presents also a higher stability due to the larger thickness of the silica walls. Usually at low pressures, the adsorption for VOCs is fairly good in micropores compared with mesopores because of the interaction between the attractive forces of the pore walls and the adsorbates (Balathanigaimani et al., 2008). Thus the longer breakthrough time for toluene adsorption on SBA-15-2 sample should be attributed to the existence of more micropores, being similar to the molecular sieving effect of NaY. Besides, its mesopore size (6.55 nm) is slightly larger than that of SBA-15-1 (5.60 nm), thus it is reasonable for us to suggest that the synergistic effect between microporous and mesoporous improves the toluene adsorption capacity.

As we all know the studies about desorption performance of adsorption materials and the interaction between the adsorbate molecules and the adsorbent are very important for its wide application. Figure 6 shows the TPD of toluene over different samples. From the TPD spectra, two parameters could be defined: the desorbed amount of toluene (the desorbed peak area) and the temperature corresponding to the major peak of desorption curve. The desorbed amount of adsorbate detected in the TPD experiment is a function of the number of adsorption sites available on the adsorbent surface, whereas the temperature of the peak can be considered as a relative measurement of the strength of the adsorbate-adsorbent interactions and the pore structures. The desorption takes place in reverse order of the strength of the adsorption sites and the adsorbate-adsorbent affinity.

The observed two peaks for NaY and only one peak for the other materials in the toluene TPD indicate the presence of at least two energetically different sites of toluene adsorption for NaY and one site for other four samples. The slit-shaped intercrystal mesopores, macropores, and cage-like structure (super-cage and β-cage) all existed in NaY sample (Scheme 1a), where the sodium cations are situated in the cages structure of the sample. The adsorption for gas molecules can be affected by steric hindrance or the "confinement effect" in a small cavity, and the former can weaken the adsorption, while the latter can enhance it (Datka et al., 1995). And the zeolites containing large amounts of H atoms show the desorption peak in the low-temperature region, while those containing large amounts of Na atoms show peak in the high-temperature region (Yoshimoto et al., 2007). The former two pores (intercrystal mesopores, macropores) showed a weak steric hindrance for organic compounds, which could make toluene desorption at a lower temperature (T_{d1} = 85°C), while a relative stronger "confinement effect" existing in the cage-like structure and a strong interaction of Na sodium with toluene molecules by π electrons results in the desorption temperature tending to higher temperature (T_{d2} = 234°C). Moreover, the desorption amount for toluene at high temperature is obviously higher than that desorbed at low temperature. The desorption temperature of toluene over the other four samples can only be found at a low temperature around 100°C, which is higher than that of the desorption peak (T_{d1} = 85°C) over NaY. This indicates that the interaction of toluene with the mesoporous materials is stronger than that of aromatic hydrocarbons in the packing pores of NaY, but weaker than in the cage-like structure. Although MCM-41 shows a relatively larger diffusion resistance in the second adsorption step during the adsorption process, its desorption temperature was much lower than the other samples in the TPD curves, which may be attributed to the week affinity of MCM-41 with toluene. After the He purge, the molecules was much easily desorbed from the adsorbed surface because the resistance produced by the accumulation of adsorbed molecules was weaken or disappeared in the ordering pores. No uniform pore structure appears in the SiO_2, the pore only existed in the exterior surface (Scheme 1d). Therefore, almost all of the VOCs adsorbed on the material were eliminated during the purge process. Also the maximum temperature (T_d) for toluene desorption over SBA-15 materials with micropore is higher than that of SiO_2 and MCM-41. The toluene molecules located in these micropores are released in the TPD experiments at higher temperatures. The presence of the micropores in the SBA-15 sample not only benefits the spread of the organic molecules, but also plays an important role in binding of molecules during the He purge before heat treatment. The desorption performance for VOCs is mainly governed by the interactions between adsorbate molecules and adsorbent surface.

Usually, the larger surface area will be in favor of the adsorption and desorption for toluene (Serrano et al., 2004). However, another phenomenon is observed in our experiments. The relations of micropores volume (V_{micro}) with the adsorption capacity of adsorbent for toluene ($q_{toluene}$) and the desorbed temperature (T_d) are clearly exhibited in Fig. 7. T_{d2} for NaY is shown in Fig. 7. The largest adsorption capacity for toluene is obtained on micro-zeolite (NaY), and the mesoporous/amousphous silica without micropores will give a decrease in the toluene adsorption capacity. However, the mesoporous silica with a special "bimodal pore system" makes a moderate adsorption capacity. The TPD results also demonstrate that, for the porous materials used here, the heating temperature of

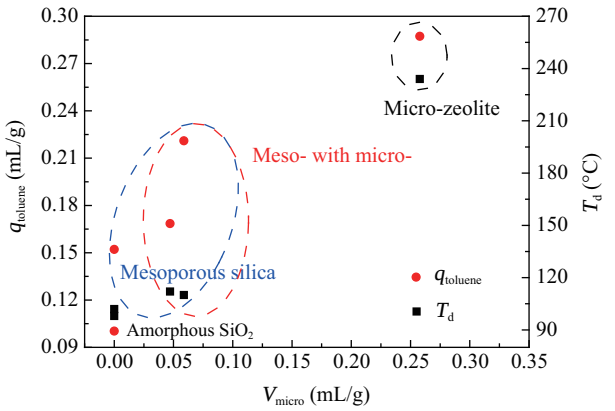

Fig. 7 Relations of micropores volume (V_{micro}) with the adsorption capacity of adsorbent for toluene ($q_{toluene}$) and the desorbed temperature (T_d).

150°C was sufficient to achieve complete elimination of VOCs on mesoporous materials (T_d of 100°C). However, the temperature needs to shift to higher temperature for the microporous materials. From the practical application point, combining the features of different materials, the mesopores are beneficial for VOCs molecules diffusion and the micropores are conducive to molecular adsorption. It will be significant to appropriately control the ratio of mesopore with micropore of adsorbents in the organic hydrocarbon removal and recycling process.

It should be also noted that the desorbed amount obtained in the TPD experiments is quite small as compared with the total adsorption capacity of each adsorbent (Table 1). Moreover the desorption amount of toluene except for NaY zeolite is decreased sharply. It has been known that only the irreversibly adsorbed adsorbate, being direct interaction with the internal pore wall, is evaluated in TPD experiments. The pore size of the samples (except for NaY) is significantly lager than the diameter of toluene molecule, which will be benefit for the molecules diffusion, and the majority toluene molecules are flowed away during He purge procedure. Therefore, an extremely lower amount of desorbed toluene than NaY is found in TPD spectra. The adsorbed toluene on the mesoporous zeolites should be easily removed during the gas flowing, and most toluene is degassed on the amorphous SiO_2 material. Also the desorption amount over mesoporous silica containing micropores is larger than the pure mesoporous material, especially for SBA-15-2 sample. The microporous structure is benefit for the adsorption of VOCs, and also makes the interaction stronger with adsorbate.

3 Conclusions

Adsorption and desorption characteristics of toluene on porous materials are investigated. There existed a strong relationship between porous structure and the adsorption and desorption performance for toluene. Microporous material NaY showed a the largest toluene adsorption amount, but its complete desorption temperature was much higher than other materials. Mesoporous MCM-41 and amorphous SiO_2 showed relatively lower adsorption capacity for toluene. SBA-15 materials with "bimodal pore system" showed a moderate adsorption capacity and desorption performance, and SBA-15 with more microporous volumes showed a better adsorption performance. The pore structure of absorbents was found to play a significant role in the adsorption properties of VOCs. The size of microporous pores, which was similar to the dynamic size of toluene, was beneficial for the adsorption of toluene, but the space resistance was larger and showed a negative effect on the desorption process. Mesoporous pores showed a positive effect on the diffusion of toluene, while the adsorption capacity of VOCs was not ideal. Thus, the significant dynamic adsorption and desorption performance should be the synergistic effect of mesopores and the large number of micropores in silica walls.

Acknowledgments

This work was supported by the National Nature Science Foundation of China (No. 20807010), the Program for New Century Excellent Talents in University (No. NCET-09-0256), the Specialized Research Fund for the Doctoral Program of Higher Education (No. 200801411111) and the National High Technology Research and Development Program (863) of China (No. 2009AA062604).

References

Agelakopoulou T, Roubani-Kalantzopoulou F, 2009. Chromatographic analysis of adsorption: chemisorption and/or physisorption. *Chromatographia*, 69(3-4): 243–255.

Akosman C, Kalender M, 2009. Analysis of diffusion and adsorption of volatile organic compounds in zeolites by a single pellet moment technique. *Clean-Soil, Air, Water*, 37(2): 115–121.

Baek S W, Kim J R, Ihm S K, 2004. Design of dual functional adsorbent/catalyst system for the control of VOC's by using metal-loaded hydrophobic Y-zeolites. *Catalysis Today*, 93-95: 575–581.

Balathanigaimani M S, Shim W G, Lee M J, Lee J W, Moon H, 2008. Adsorption isotherms of benzene and toluene on corn grain-based carbon monolith at (303.15, 313.15, and 323.15) K. *Chemical Engineering Data*, 53(3): 732–736.

Cheng H F, Reinhard M, 2006. Sorption of trichloroethylene in hydrophobic micropores of dealuminated Y zeolites and natural minerals. *Environmental Science & Technology*, 40(24): 7694–7701.

Choudhary V R, Srinivasan K R, Singh A P, 1990. Temperature-programmed desorption of aromatic hydrocarbons on silicalite-I and ZSM-5-type zeolites. *Zeolites*, 10(1): 16–20.

Datka J, Boczar M, Gil B, 1995. Heterogeneity of hydroxyl groups in zeolites studied by IR spectroscopy. *Colloids and Surfaces A: Physicochemical and Engineering Aspects*, 105(1): 1–18.

Delhoménie M C, Heitz M, 2005. Biofiltration of air: A review. *Critical Reviews Biotechnology*, 25(1-2): 53–72.

Galarneau A, Cambon H, Renzo F D, Ryoo R, Choi M, Fajula F, 2003. Microporosity and connections between pores in SBA-15 mesostructured silicas as a function of the temperature of synthesis. *New Journal of Chemistry*, 27: 73–79.

Ghorai P K, 2010. Conformational preferences of *n*-Butane inside zeolite NaY: comparison of other related properties

with *iso*-Butane. *Journal of Physical Chemistry B*, 114(19): 6492–6499.

Gregg S J, Sing K S W, 1982. Adsorption Surface Area and Porosity (2nd ed.). Academic Press, New York. 1–303.

Guillemot M, Mijoin J, Mignard S, Magnoux P, 2007. Adsorption of tetrachloroethylene on cationic X and Y zeolites: influence of cation nature and of water vapor. *Industrial & Engineering Chemistry Research*, 46(13): 4614–4620.

Hu Q, Li J J, Hao Z P, Li L D, Qiao S Z, 2009. Dynamic adsorption of volatile organic compounds on organofunctionalized SBA-15 materials. *Chemical Engineering Journal*, 149(1-3): 281–288.

Hu Q, Li J J, Qiao S Z, Hao Z P, Tian H, Ma C Y et al., 2009. Synthesis and hydrophobic adsorption properties of microporous/mesoporous hybrid materials. *Journal of Hazardous Materials*, 164(2-3): 1205–1212.

Hu X J, Qiao S Z, Zhao X S, Lu G Q, 2001. Adsorption study of benzene in ink-bottle-like MCM-41. *Industrial & Engineering Chemistry Research*, 40(3): 862–867.

Huang Y, Wang K, Dong D H, Li D, Hill M R, Hill A J et al., 2010. Synthesis of hierarchical porous zeolite NaY particles with controllable particle sizes. *Microporous and Mesoporous Materials*, 127(3): 167–175.

Impéror-Clerc M, Davidson P, Davidson A, 2000. Existence of a microporous corona around the mesopores of silica-based SBA-15 materials templated by triblock copolymers. *Journal of the American Chemical Society*, 122(48): 11925–11933.

Kosuge K, Kubo S, Kikukawa N, Takemori M, 2007. Effect of pore structure in mesoporous silicas on VOC dynamic adsorption/desorption performance. *Langmuir*, 23(6): 3095–3102.

Lillo-Ródenas M A, Carratalá-Abril J, Cazorla-Amorós D, Linares-Solano A, 2002. Usefulness of chemically activated anthracite for the abatement of VOC at low concentrations. *Fuel Process Technology*, 77-78: 331–336.

Marti' J, Soria J, Cano F H, 1977. Cation location in hydrated NaY zeolites. *Journal of Colloid and Interface Science*, 60(1): 82–86.

Otremba M, Zajdel W, 1993. Temperature-programmed desorption of n-propylbenzene from HNaZSM-5 and Na(Li, K, Rb, Cs) ZSM-5 type zeolites. *Reaction Kinetics and Catalysis Letters*, 51(2): 481–487.

Piwonski I, Zajac J, Jones D J, Rozière J, Partyka S, Plaza S, 2000. Adsorption of influence from toluene solutions on MCM-41 silica: A flow microcalorimetric study. *Langmuir*, 16(24), 9488–9492.

Ravikovitch P I, Vishnyakov A, Neimark A V, Manuela M L, Carrott R, Russo P A et al., 2006. Characterization of micro-mesoporous materials from nitrogen and toluene adsorption: Experiment and modeling. *Langmuir*, 22(2): 513–516.

Russo P A, Carrott M M L R, Carrott P J M, 2008. Adsorption of toluene, methylcyclohexane and neopentane on silica MCM-41. *Adsorption*, 14(2-3): 367–375.

Ryoo R, Ko C H, Michal K, Antochshuk V, Jaroniec M, 2000. Block-copolymer-templated ordered mesoporous silica: array of uniform mesopores or mesopore-micropore network? *Journal of Physical Chemistry B*, 104(48): 11465–11471.

Serrano D P, Calleja G, Botas J A, Gutierrez F J, 2004. Adsorption and hydrophobic properties of mesostructured MCM-41 and SBA-15 materials for volatile organic compound removal. *Industrial & Engineering Chemistry Research*, 43(22): 7010–7018.

Su B L, Norberg V, 2000. Location of Benzene in NaBeta zeolite upon coadsorption of ammonia and methylamine: A further confirmation of molecular recognition effect in benzene adsorption in 12R window zeolites. *Langmuir*, 16(14): 6020–6028.

Szegedi Á, Popova M, Minchev C, 2009. Catalytic activity of Co/MCM-41 and Co/SBA-15 materials in toluene oxidation. *Journal of Materials Science*, 44(24): 6710–6716.

Tong W Y, Kong D J, Liu Z C, Guo Y L, Fang D Y, 2008. Synthesis and characterization of ZSM-5/silicalite-1 core-shell zeolite with a fluoride-containing hydrothermal system. *Chinese Journal of Catalysis*, 29(12): 1247–1252.

Wang J, Xu F, Xie W J, Mei Z J, Zhang Q Z, Cai J et al., 2009. The enhanced adsorption of dibenzothiophene onto cerium/nickel-exchanged zeolite Y. *Journal of Hazardous Materials*, 163(2-3): 538–543.

Yao M, Zhang Q, Hand D W, Perram D, 2009. Adsorption and regeneration on activated carbon fiber cloth for volatile organic compounds at indoor concentration levels. *Journal of the Air and Waste Management Association*, 59(1): 31–36.

Yoshimoto R, Hara K, Okumura K, Katada N, Niwa M, 2007. Analysis of toluene adsorption on Na-form zeolite with a temperature-programmed desorption method. *The Journal of Physical Chemistry C*, 111(3): 1474–1479.

Zhao D Y, Feng J L, Huo Q S, Melosh N, Frendrickson G H, Chmelka B F et al., 1998. Triblock copolymer syntheses of mesoporous silica with periodic 50 to 300 angstrom pores. *Science*, 279(5350): 548–552.